nature biotechnology

Single-base resolution analysis of active DNA demethylation using methylase-assisted bisulfite sequencing

Hao Wu[1–5], Xiaoji Wu[1–5], Li Shen[1–4] & Yi Zhang[1–4]

Active DNA demethylation in mammals involves TET-mediated iterative oxidation of 5-methylcytosine (5mC)/5-hydroxymethylcytosine (5hmC) and subsequent excision repair of highly oxidized cytosine bases 5-formylcytosine (5fC)/5-carboxylcytosine (5caC) by thymine DNA glycosylase (TDG). However, quantitative and high-resolution analysis of active DNA demethylation activity remains challenging. Here, we describe M.SssI methylase-assisted bisulfite sequencing (MAB-seq), a method that directly maps 5fC/5caC at single-base resolution. Genome-wide MAB-seq allows systematic identification of 5fC/5caC in *Tdg*-depleted embryonic stem cells, thereby generating a base-resolution map of active DNA demethylome. A comparison of 5fC/5caC and 5hmC distribution maps indicates that catalytic processivity of TET enzymes correlates with local chromatin accessibility. MAB-seq also reveals strong strand asymmetry of active demethylation within palindromic CpGs. Integrating MAB-seq with other base-resolution mapping methods enables quantitative measurement of cytosine modification states at key transitioning steps of the active DNA demethylation cascade and reveals a regulatory role of 5fC/5caC excision repair in this step-wise process.

DNA methyltransferases (DNMTs) chemically modify the genome by adding a methyl group to the 5-position of cytosines[1], generating an epigenetic mark (5mC) that has a profound impact on genome stability, transcription and development[2,3]. Dysregulation of 5mC patterns is frequently associated with human cancers[4]. Compelling evidence now indicates that reversal of DNA methylation plays an important role in mammalian development and cell type–specific gene expression. In mammals, DNA demethylation (conversion of 5mC to unmodified C) can be achieved either passively through successive rounds of DNA replication in the absence of functional DNA methylation maintenance machinery or actively by the Ten-eleven translocation (TET) family of 5mC-modifying enzymes[5,6]. TET proteins are Fe^{2+}- and 2-oxoglutarate–dependent dioxygenases capable of successively oxidizing 5mC to 5hmC, 5fC and 5caC (**Fig. 1a**)[7–10]. Oxidative modification of 5mC by TET enzymes promotes DNA demethylation by either replication-dependent dilution of oxidized cytosines[11] or TDG-mediated 5fC/5caC excision followed by base-excision repair (BER)[10,12,13]. The active demethylation pathway involving generation and excision repair of 5fC/5caC is of particular interest as it may take place in a wide range of somatic cell types including postmitotic cells. Interestingly, only TDG, but not other members of the uracil DNA glycosylase superfamily, possesses robust 5fC/5caC excision activity and is indispensable for embryonic development[14,15], implicating the TET/TDG-dependent DNA demethylation pathway in regulating tissue-specific gene expression and development.

The observation that 5hmC can accumulate to a relatively high level in diverse cell types, particularly in adult neurons[16,17], raises the possibility that TET proteins tend to stall at 5hmC and that further oxidation of 5hmC to 5fC/5caC is a rate-limiting step. Therefore, identifying cytosines that are committed to active DNA demethylation requires methods that permit quantitative measurement of TDG-mediated excision of 5fC/5caC at high resolution. In addition, because both 5fC and 5caC are selectively recognized and excised by TDG, determining the strand-specific preference of active DNA demethylation activity requires the ability to simultaneously map both 5fC and 5caC. Recent studies using either 5fC/5caC-specific antibodies or chemical tagging of 5fC have shown that genomic regions containing cytosines undergoing TET/TDG-dependent active demethylation can be identified by analyzing ectopic 5fC/5caC accumulation in *Tdg*-depleted cells[18,19]. However, 5fC and 5caC maps generated by affinity-enrichment methods are of limited resolution (several hundred base-pairs), represent only relative enrichment and lack strand distribution information. To address these limitations, we have developed a method named MAB-seq, which allows simultaneous and quantitative mapping of both 5fC and 5caC at base resolution. Furthermore, our genome-wide MAB-seq analysis of mouse embryonic stem cells (ESCs) has provided new insights into catalytic processivity, strand asymmetry and feedback regulation of the TET/TDG-mediated active DNA demethylation pathway.

[1] Howard Hughes Medical Institute, Boston, Massachusetts, USA. [2] Program in Cellular and Molecular Medicine, Boston Children's Hospital, Boston, Massachusetts, USA. [3] Harvard Stem Cell Institute, Boston, Massachusetts, USA. [4] Department of Genetics, Harvard Medical School, Boston, Massachusetts, USA.
[5] These authors contributed equally to this work. Correspondence should be addressed to Y.Z. (yzhang@genetics.med.harvard.edu) or H.W. (haowu7@gmail.com).

Received 14 June; accepted 15 October; published online 2 November 2014; doi:10.1038/nbt.3073

RESULTS

Experimental strategy and validation of MAB-seq

Recognizing the limitation of affinity-enrichment methods and several recently developed chemical modification–assisted bisulfite (BS)-seq methods that require subtraction of BS-seq signals to indirectly map 5fC or 5caC[19–21] (**Supplementary Fig. 1a**), we have explored MAB-seq, an approach that aims to achieve direct and simultaneous measurement of 5fC and 5caC at single-base resolution (**Fig. 1a**). In standard BS-seq, C/5fC/5caC reacts with sodium bisulfite and are efficiently deaminated to uracil (C/5fC) or 5caU (5caC), both of which are sequenced as thymine (T), whereas 5mC and 5hmC are resistant to this chemical conversion and sequenced as C (**Fig. 1a**). In MAB-seq, genomic DNA is first treated with the bacterial DNA CpG methyltransferase M.SssI, an enzyme that is originally isolated from *Spiroplasma sp.* strain MQ1 and is known to efficiently methylate cytosines within CpG dinucleotides[22]. Bisulfite conversion of M.SssI-treated DNA may therefore only deaminate 5fC and 5caC; originally unmodified C within CpGs is protected as 5mC. Subsequent sequencing would reveal 5fC and 5caC as T, whereas C/5mC/5hmC would be sequenced as C (**Supplementary Fig. 2a**). Notably, MAB-seq is unable to distinguish 5fC/5caC from unmodified C within a non-CpG context due to the poor activity of M.SssI toward C within a non-CpG context. This limitation does not affect the application of this technique for two reasons: first, 5hmC is found almost exclusively in the CpG context (>99% in CpGs), even in mouse ESCs and neurons where non-CpG methylation is prevalent[17,23]; second, recent structural and biochemical analyses indicate that TET proteins have a strong preference for oxidizing 5mC in CpG sites than in non-CpG context[24,25]. Thus, oxidative modification of 5mC by TET proteins occurs predominantly in the CpG context, and MAB-seq may provide a quantitative measurement of the abundance of 5fC/5caC within CpG dyads.

Successful detection of 5fC/5caC using MAB-seq requires complete conversion of C to 5mC by M.SssI as well as efficient bisulfite conversion of 5fC/5caC. We first optimized the reaction conditions and achieved nearly complete (99.2%) conversion of unmodified CpGs to 5mCpGs by M.SssI methylase measured by Sanger sequencing (**Supplementary Fig. 1b**). Next, we performed high-throughput BS-seq analysis of a synthetic double-stranded DNA (dsDNA) containing CpGs with specific cytosine modifications (5hmC/5fC/5caC). Consistent with previous reports[21], our analysis showed that 5fC (84.7%) and 5caC (99.5%), but not 5hmC (3.3%), are efficiently deaminated by bisulfite treatment and read as T (**Supplementary Fig. 2b**). In addition to unmodified CpGs (C:C), asymmetrically modified CpGs may be present at low levels in the genome[23]. We thus tested MAB-seq in analyzing asymmetrically modified dsDNA (5hmC/5fC/5caC:C). This analysis demonstrated that M.SssI methylase is capable of efficiently methylating unmodified C in hemi-modified CpG dyads (**Supplementary Fig. 2c**), validating the capability of MAB-seq in mapping asymmetrically modified 5fC/5caC in a strand-specific manner.

We next performed BS-seq and MAB-seq analysis of the unmethylated lambda phage genome (6,224 CpGs within 48,502 bp) using Illumina high-throughput sequencing and sequenced to an average depth of 239× and 305× per cytosine, respectively. In BS-seq, a nearly

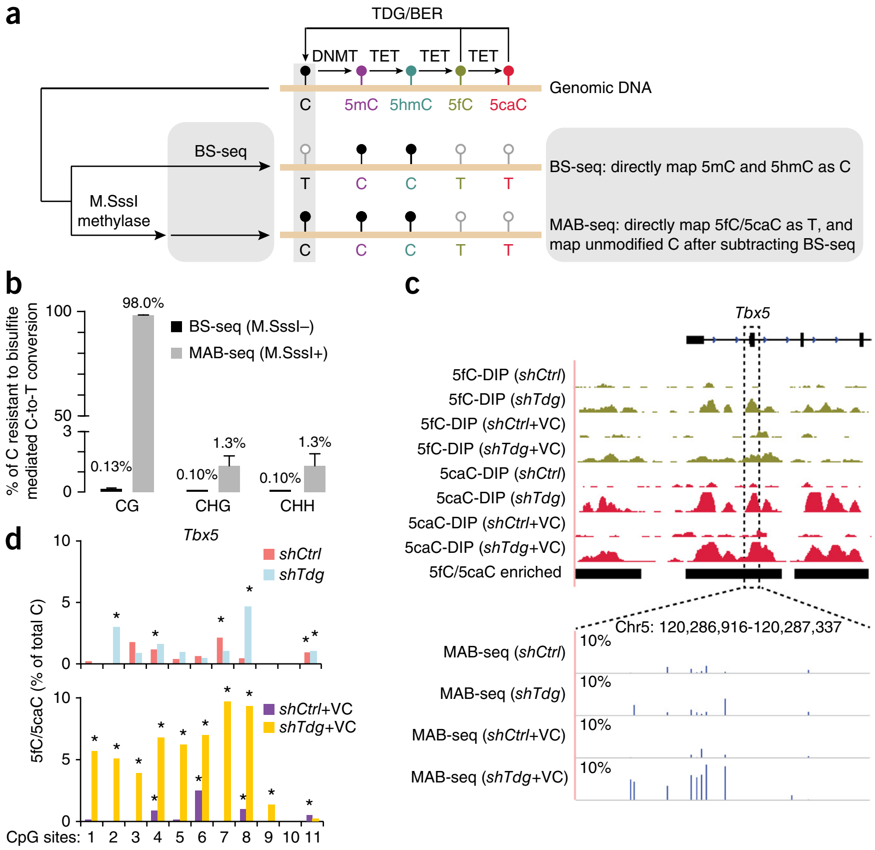

Figure 1 MAB-seq strategy and quantitative mapping of active DNA demethylation. (**a**) Schematic diagram of MAB-seq. DNMT methylates unmodified C to generate 5mC, which can be successively oxidized by TET to generate 5hmC/5fC/5caC. Highly oxidized cytosine derivatives, 5fC and 5caC, are repaired by TDG/BER to regenerate unmodified C. (**b**) M.SssI exhibits robust methylase activity toward unmodified cytosines within CpGs, but has substantially lower activity for cytosines in non-CpG contexts (CHG or CHH, H = A, T, C). M.SssI methylase activity was measured by MAB-seq analysis (Illumina deep sequencing) of unmethylated lambda DNA. Standard BS-seq confirmed nearly complete conversion of unmethylated C to T at CpG and non-CpG sites. Error bars, s.e.m. (**c**) Locus-specific MAB-seq analysis of 5fC/5caC at *Tbx5* by Illumina sequencing in control (*shCtrl*) and *Tdg* knockdown (*shTdg*) mouse ESCs. For comparison, also shown are 5fC/5caC antibody DIP-based maps of 5fC and 5caC in control and *Tdg*-depleted mouse ESCs. DIP-seq tracks are represented in normalized read density (reads per 10 million reads) and the vertical axis range of all DIP-seq tracks is from 1 to 25. Black horizontal bars denote 5fC/5caC-enriched regions identified by 5fC/5caC DIP-seq. The level of 5fC/5caC (only Watson strand shown) is displayed as the percentage of total C modified as 5fC/5caC, and background signals detected in *Tet1/2*$^{-/-}$ mouse ESCs were subtracted. (**d**) Statistical calling of 5fC/5caC-modified CpGs in locus-specific MAB-seq analysis. Shown are 5fC/5caC levels (background corrected using raw MAB-seq signals in *Tet1/2*$^{-/-}$) of 11 CpG sites from the *Tbx5* locus in *shCtrl*, *shCtrl*+VC, *shTdg* and *shTdg*+VC mouse ESCs. An asterisk indicates that a CpG is statistically enriched for 5fC/5caC (multiple comparison corrected $P < 0.05$, Fisher's exact test).

complete C-to-T conversion within CpG sites was observed (99.9 ± 0.06%, n = 3 experiments) contrasted to a low conversion rate in MAB-seq (2.04 ± 0.14%, n = 9) (**Fig. 1b** and **Supplementary Fig. 3a**). To test whether unprotected CpGs in MAB-seq experiments exhibit random distribution, we analyzed the sequences immediately flanking 67 CpGs (mean methylation: 94.1%) that are not efficiently methylated by M.SssI (**Supplementary Fig. 3b**,**c**). We found that these 67 CpGs are not associated with any specific sequences (**Supplementary Fig. 3d**), suggesting that M.SssI has minimal sequence preference for catalyzing CpG methylation reactions. Consistent with previous findings[22], we found that M.SssI methylates only a small fraction of cytosines (1.3%) within non-CpG context (**Fig. 1b** and **Supplementary Fig. 3a**).

To test MAB-seq in analyzing mammalian genomic DNA, we applied this method to examine four 5fC/5caC-enriched loci (*Tbx5*, *Vps26a*, *Ace* and *Slc2a12*) that were previously identified in *Tdg*-depleted mouse ESCs by affinity-enrichment methods[18,19] (**Fig. 1c**, **Supplementary Figs. 4** and **5a**). Using mouse ESCs deficient for both Tet1 and Tet2 (largely absent of 5fC/5caC) as a negative control to correct background signals, locus-specific MAB-seq analysis not only located individual CpGs associated with significant levels of 5fC/5caC (**Fig. 1d** and **Supplementary Fig. 6**; $P < 0.05$, Fisher's exact test), but also revealed the absolute level of 5fC/5caC at each CpG (**Fig. 1c** and **Supplementary Fig. 4**). This analysis also confirmed the positive effect of vitamin C (VC) on the catalytic activity of TET enzymes[26,27], as VC-treated *Tdg*-depleted mouse ESCs (*shTdg* + VC) displayed even higher levels of 5fC/5caC compared to *shTdg* cells (**Fig. 1c** and **Supplementary Figs. 4** and **6**). Notably, a small number of 5fC/5caC-modified CpGs were also identified in the *shCtrl* and *shCtrl* + VC samples (**Fig. 1d** and **Supplementary Fig. 6**). Although the levels of 5fC/5caC in *shCtrl* are much lower than those in *shTdg*, the results suggest that MAB-seq is highly sensitive and may identify rare 5fC/5caC modifications in wild-type cells. Similar 5fC/5caC distribution patterns were detected for biologically independent replicates, demonstrating the reproducibility and robustness of MAB-seq (**Supplementary Fig. 5b**).

Genome-wide MAB-seq analysis of mouse ESCs

Having validated MAB-seq using locus-specific analysis, we next applied MAB-seq to identify cytosines undergoing active DNA demethylation at the genome scale (**Fig. 2**). Affinity enrichment–based studies of 5fC/5caC distributions in mouse ESCs have shown that a large cohort of 5fC and 5caC peaks overlap with genomic regions enriched for H3K4me1 (refs. 18,19), a histone mark broadly associated with active/poised enhancers, flanking regions of active/poised gene promoters, and intragenic regions of actively transcribed genes[28]. Because H3K4me1-marked regions enrich for 5fC/5caC signals, we focused our initial genome-scale MAB-seq analysis on H3K4me1-enriched genomic regions captured through chromatin immunoprecipitation (termed H3K4me1-MAB-seq) (**Supplementary Fig. 7a**). To establish the baseline of false-positive 5fC/5caC signals, we performed H3K4me1-MAB-seq analysis of mouse ESCs deficient for all three Dnmt enzymes (*Dnmt1/3a/3b*$^{-/-}$) or Tet1/2 proteins (*Tet1/2*$^{-/-}$). We found that median false-positive signals in these mutant ESCs, in which both 5fC and 5caC are virtually absent, are very close to the error rate of M.SssI observed in methylating lambda DNA (dashed line in **Fig. 2b**). In comparison to control knockdown (*shCtrl*), *Dnmt1/3a/3b*$^{-/-}$, *Tet1/2*$^{-/-}$ ESCs, 5fC/5caC is present at significantly higher levels in *Tdg* knockdown (*shTdg*) mouse ESCs ($P < 2.2 \times 10^{-16}$, Wilcoxon rank sum test), and is further increased in VC-treated cells (*shTdg*+VC in **Fig. 2b**).

Given that 5fC/5caC is absent in *Dnmt*/*Tet* mutant (denoted as 'Neg Ctrl' hereafter) mouse ESCs, MAB-seq signals in these mutant cells may provide an empirical estimate of the false-discovery rate (FDR). Because the probability that a CpG can be confidently identified as 5fC/5caC-modified is governed by the sequencing depth and abundance of the modification at the cytosine, we modeled the largely stochastic event of M.SssI failure in CpG methylation with a binomial distribution (N as the depth of sequencing at the cytosine and P (2.04%) as the error rate of M.SssI). Application of this statistical strategy to H3K4me1-MAB-seq data sets identified a total of 127,576 (7.6% out of 1,670,036 CpG dyads with $N \geq 10$) 5fC/5caC-modified CpG dyads in VC-treated, *Tdg*-depleted mouse ESCs (*shTdg*+VC) with an empirical FDR of 5%. Using a less stringent cutoff ($N \geq 5$, FDR<10%), we have identified 267,325 (8.0% out of 3,326,034 CpG dyads) 5fC/5caC-modified CpGs. There are 17.6 times as many 5fC/5caC-modified CpGs (in *shTdg*+VC) overlapping with affinity-identified regions as in negative controls (**Fig. 2c**), demonstrating the effectiveness of the empirical FDR-based statistical filter.

We next analyzed genomic DNA from mouse ESCs by whole genome (WG)-MAB-seq. Since VC is present at a relatively high level during early development *in vivo*[29], base-resolution 5fC/5caC map in VC-treated cells may represent a more physiologically relevant profile of TET/TDG-dependent active demethylation activity. We therefore focused our WG-MAB-seq analysis on *shTdg*+VC mouse ESCs and sequenced the sample to an average depth of 28.4× per CpG dyad (covering 95.2% of all CpG dyads). Locus-specific analysis of nonenriched and H3K4me1-enriched DNA suggests that 5fC/5caC levels at specific CpGs within selected loci are largely comparable (**Supplementary Fig. 7b**,**c**). Further comparative analysis of both H3K4me1-MAB-seq and WG-MAB-seq experiments indicates that MAB-seq signals (T/C+T) are highly similar in both experiments at a wide range of promoter-proximal and distal genomic elements (**Supplementary Fig. 8a**), supporting the validity of using the statistical filter established for H3K4me1-MAB-seq to analyze the WG-MAB-seq data set. Using the empirical P value cutoff established for H3K4me1-MAB-seq data sets with comparable sequencing depth, we identified a total of 675,325 5fC/5caC-modified CpGs (out of 24,872,637 CpGs ($N \geq 10$)) in *shTdg*+VC mouse ESCs through WG MAB-seq analysis (with an empirical FDR of 5%). Identified 5fC/5caC-modified CpGs in *Tdg*-depleted cells correlate well with peaks of 5fC and 5caC enrichment identified by the antibody-based DNA immunoprecipitation (DIP) approach (region 1 in **Fig. 2a**). Compared to random controls, 5fC/5caC-CpGs significantly overlapped with 5fC/5caC-enriched peaks (7.9 times as many as expected by chance, Z-score = 579.3). Furthermore, 83.6% of affinity enrichment–identified regions (n = 50,923 out of 60,912 covered by WG-MAB-seq) overlapped with at least one 5fC/5caC-modified CpGs. By contrast, as exemplified by region 2 in **Figure 2a**, 80.7% of 5fC/5caC-modified CpGs were not recovered by 5fC/5caC DIP-seq (region 2 in **Fig. 2**), suggesting that MAB-seq has a markedly increased sensitivity.

Genomic distribution of active DNA demethylation activity

Previous studies using affinity enrichment–based methods have shown that 5fC/5caC are enriched at poised and/or active enhancers, Polycomb group protein (PcG) repressed promoters, and gene bodies[18,19]. However, the true abundance of 5fC/5caC cannot be determined from affinity-based approaches, thus precluding quantitative analysis of 5fC/5caC-excision-dependent DNA demethylation events at these gene regulatory elements. In *shTdg*+VC mouse ESCs, we found that a considerable fraction of 5fC/5caC (20.1%) reside in distal regulatory regions (**Fig. 2d**). Analysis of both raw MAB-seq signals and relative enrichment of called 5fC/5caC at each class of genomic features indicates that 5fC/5caC are more enriched at DNase I hypersensitive sites (observed/random (obs/rand) = 5.2), predicted enhancers (obs/rand = 4.6), and CTCF-biding sites (obs/rand = 2.4) relative to promoter-proximal regions and other genic regions (**Fig. 2e** and **Supplementary Fig. 8c,d**). In support of this observation, regions enriched for pluripotency-related transcription factors (Oct4, Nanog and Sox2) as well as active enhancers (marked by H3K27ac and/or H3K4me1) are also more enriched with 5fC/5caC than with other genomic elements (**Fig. 2f** and **Supplementary Fig. 8b**). Consistent with previous reports[18,19], we found that 5fC/5caC was more enriched at mouse ESC-specific distal enhancers than at other tissue-specific enhancers (**Supplementary Fig. 8e,f**), supporting the notion that CpGs within or surrounding active cell-type-specific

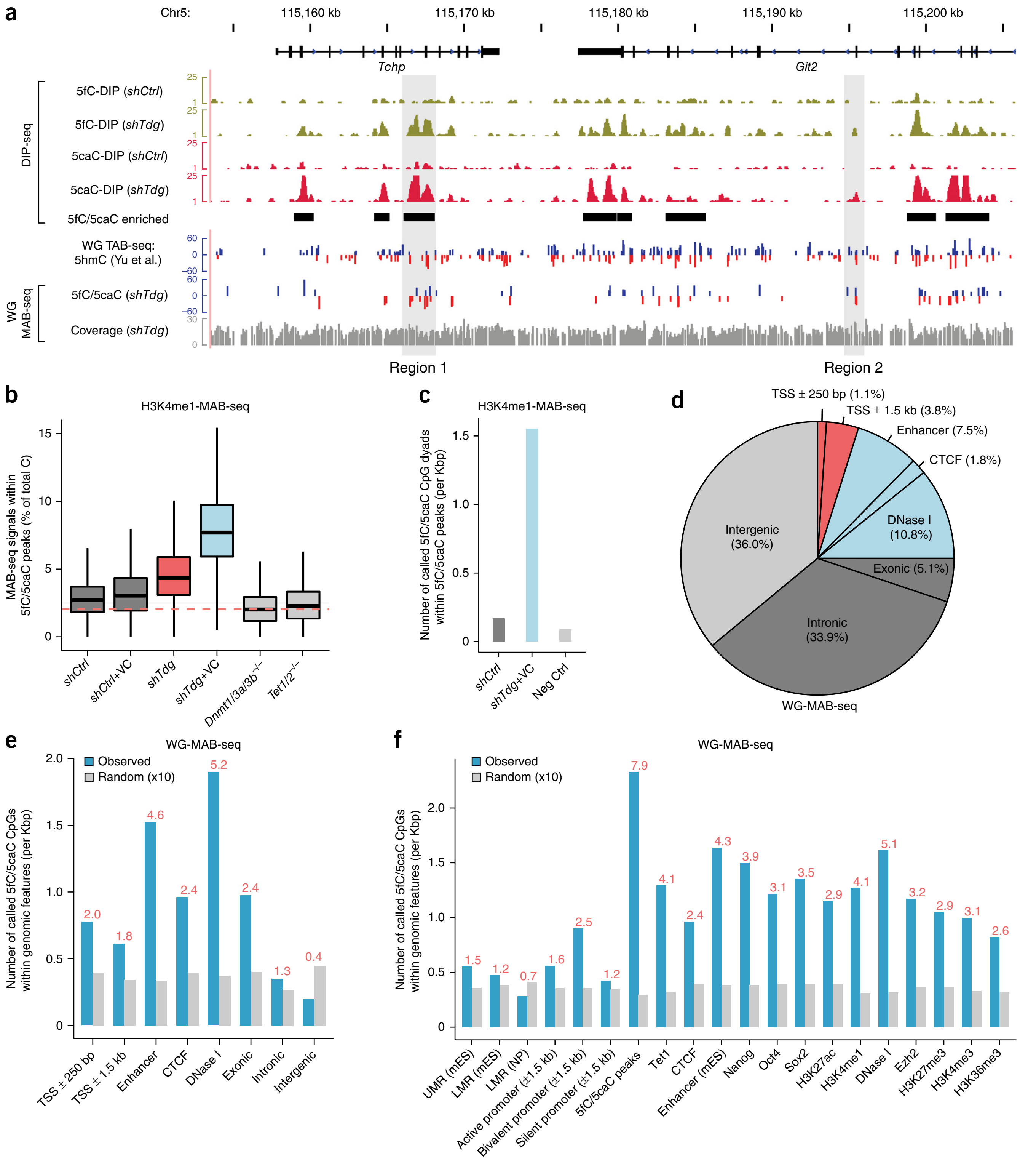

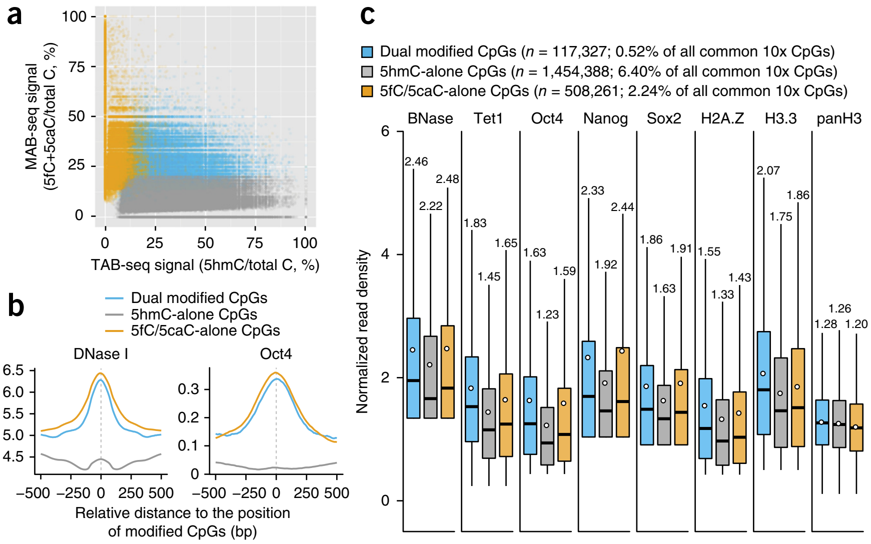

Figure 3 Identification of CpGs associated with distinct processivity of TET-mediated oxidation. (**a**) Comparative analysis of base-resolution 5fC/5caC (WG-MAB-seq in *shTdg*+VC) and 5hmC maps (TAB-seq in wild type)[23] identifies CpGs associated only with 5fC/5caC (5fC/5caC-alone; *n* = 508261, FDR = 5%), 5hmC (5hmC-alone; *n* = 1,454,388, FDR = 5%) and both (dual modified with 5hmC and 5fC/5caC; *n* = 117,327, FDR = 5%). 5fC/5caC-alone CpGs (yellow), which are only associated with generation and excision repair of 5fC/5caC, represent cytosines undergoing active DNA demethylation; 5hmC-alone CpGs (gray), which are only associated with relatively stable 5hmC in wild-type cells, represent cytosines where TET proteins tend to stall at 5hmC; dual-modified CpGs (blue), which are associated with active demethylation but 5hmC also accumulates to detectable level in wild-type cells. The levels of MAB-seq and TAB-seq signals are depicted in the scatter plot for all CpGs (*n* = 22,730,906) that are covered by both MAB-seq (depth ≥ 10) and TAB-seq (depth ≥ 10). (**b**) Averaged read density of DNase I hypersensitivity signals (left panel; averaged from two DNase-seq replicates) and Oct4 ChIP-seq (right panel; whole cell extract (WCE) control ChIP-seq signal subtracted) around 5hmC-alone CpGs, 5fC/5caC-alone and dual-modified CpGs (±500 bp). (**c**) The levels of chromatin accessibility signals (BNase), TET1 occupancy, pluripotency transcriptional factors (Nanog, Oct4 and Sox2) and histone variants (H2A.Z and H3.3) around the genomic position (±50 bp) of indicated groups of modified CpGs. The black bars and white circles in boxplots denote median and mean of normalized read density (reads per 10 million reads). The mean of each boxplot is shown on the top.

enhancers tend to undergo 5fC/5caC-excision-dependent active DNA demethylation.

Distinct processivity of TET enzymes at different cytosines

The ability of identifying individual CpGs undergoing 5fC/5caC-excision-dependent DNA demethylation offers an opportunity for investigating the processivity of TET-mediated 5mC oxidation. We thus focused on CpGs sufficiently covered by both the WG 5fC/5caC map (in *shTdg*+VC) and 5hmC map generated by TAB-seq[23] (**Fig. 2a**). Comparative analysis of TAB-seq and WG-MAB-seq signals (depth ≥10) allows us to estimate the number of CpGs associated with 5fC/5caC-alone (5hmC$^-$, 5fC/5caC$^+$; *n* = 508,261), 5hmC-alone (5hmC$^+$, 5fC/5caC$^-$; *n* = 1,454,388), and both (5hmC$^+$, 5fC/5caC$^+$; *n* = 117,327) (**Fig. 3a**). The median raw MAB-seq signal at 5fC/5caC-alone CpGs is 23.1%, substantially higher than 5.6% detected for 5hmC-alone CpGs (**Supplementary Fig. 9a**). Notably, 5hmC and 5fC/5caC largely exist at different cytosines (**Fig. 3a**). Only 7.5% of 5hmC-modified CpGs (depth≥10) also had significant levels of 5fC/5caC (corresponding to 18.8% of all 5fC/5caC-modified CpGs, FDR = 5%), whereas the majority of 5hmC-modified CpGs appeared to represent 5hmC stably accumulated in wild-type cells without being efficiently further oxidized by TET proteins to 5fC/5caC (pair #1 in **Supplementary Fig. 9b**). Additional analysis using CpGs with higher sequencing depth (depth ≥ 20) reached similar conclusion (pair #2 in **Supplementary Fig. 9b**). In contrast, affinity-based 5hmC/5fC/5caC mapping methods suggest a much higher overlapping percentage

Figure 2 Genome-scale MAB-seq analysis of the mouse genome. (**a**) Snapshot of base-resolution 5fC/5caC maps (in *shTdg*+VC) and affinity-based 5fC/5caC maps at the *Tchp-Git2* locus in wild-type or *Tdg*-depleted mouse ESCs compared to the base-resolution 5hmC map (TAB-seq)[23] in wild-type ESCs. For comparison, 5fC/5caC-enriched regions (*shTdg*-specific) identified by DIP-seq methods are highlighted by black horizontal bars. For base-resolution maps, positive values (blue) indicate cytosines on the Watson strand, whereas negative values (red) indicate cytosines on the Crick strand. For base-resolution maps of 5hmC and 5fC/5caC, the vertical axis limits are –60% to +60%. Only cytosines sequenced to depth ≥5 are shown. Cytosines associated with statistically significant level of 5hmC (FDR = 5%) and 5fC/5caC (FDR = 5%) are shown in separate tracks. Sequencing coverage for WG-MAB-seq experiments is shown in gray. (**b**) Genome-scale H3K4me1-MAB-seq analysis confirms that TDG inactivation and/or VC treatment resulted in higher 5fC/5caC levels. Shown are boxplots of raw MAB-seq signals (percentage of T/(C+T)) mapped to 5fC/5caC-enriched regions (*n* = 51,235; covered cytosines ≥20; identified by 5fC/5caC antibody DIP-seq). *Dnmt1/3a/3b*$^{-/-}$ and *Tet1/2*$^{-/-}$ mouse ESCs served as negative controls. The dashed line denotes the error rate for M.SssI methylase (2.04%). *shCtrl*, control knockdown mouse ESCs; *shCtrl*+VC, control knockdown and VC-treated mouse ESCs; *shTdg*, TDG knockdown mouse ESCs; *shTdg*+VC, TDG knockdown and VC-treated mouse ESCs. (**c**) Statistical analysis of H3K4me1-MAB-seq data sets (depth ≥5, FDR < 10%) identifies specific CpG dyads enriched for 5fC/5caC. Shown are the number of called cytosines within 5fC/5caC-enriched regions for control, sh*Tdg*+VC, and Neg Ctrl. *shCtrl*, denotes merged MAB-seq data sets from *shCtrl* and *shCtrl*+VC samples. Neg Ctrl denotes merged MAB-seq data sets from *Dnmt1/3a/3b*$^{-/-}$ and *Tet1/2*$^{-/-}$ samples. (**d**) Overlap of 5fC/5caC-modified CpGs (FDR = 5% in WG-MAB-seq analysis of *shTdg*+VC sample) with genomic elements. Genic features were extracted from the UCSC RefGene database (mm9). Promoter-distal regulatory regions (e.g., enhancers, CTCF binding sites and DNase I hypersensitive regions) were experimentally mapped by ChIP-seq and DNase-seq experiments of the ENCODE project[30]. Each 5fC/5caC is counted only once: the overlap of a genomic region excludes all previously overlapped cytosines clockwise from proximal promoters (TSS ± 250 bp). Red, promoter-proximal regions; blue, promoter-distal regulatory elements; dark gray, genic regions; light gray, intergenic regions. (**e**) The relative enrichment of 5fC/5caC-modified CpGs at genomic elements (blue) and corresponding randomly shuffled control regions (gray), normalized to the total size of the element type (per kilo base-pairs (Kbp)). Random consists of 10 random shuffling of specific genomic elements in the mouse genome. The ratio between observed and random for each genomic element is shown on the top (red). (**f**) The relative enrichment of 5fC/5caC-modified CpGs at specific gene regulatory regions (blue) and corresponding randomly shuffled control regions (gray). 5fC/5caC peaks, 5fC/5caC-enriched regions identified by DIP-seq. UMR, unmethylated region, typically marking transcriptionally active CpG-rich promoters; LMR, low methylation region. mES, mouse ESCs; NP, neural progenitors.

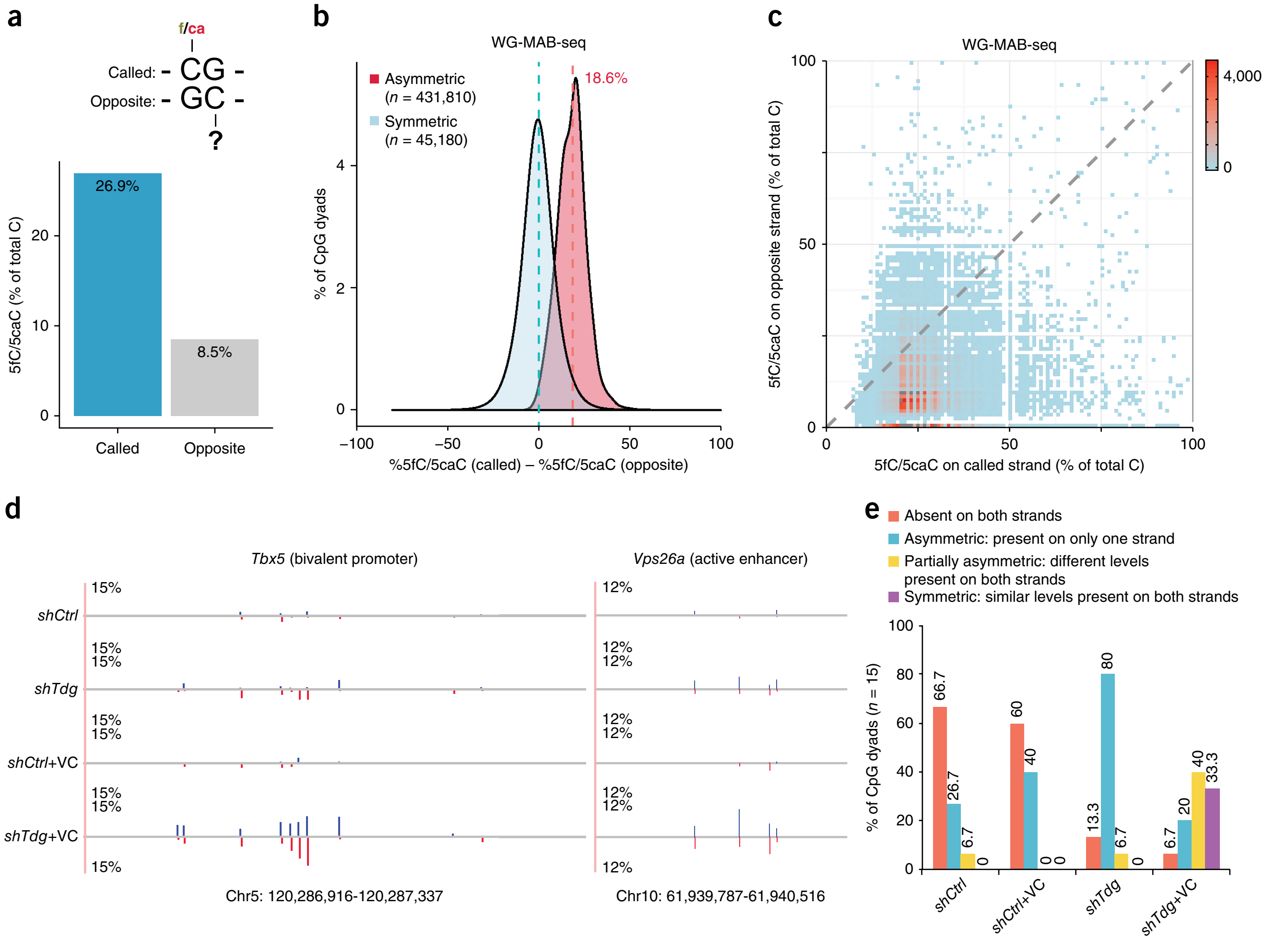

Figure 4 Strand asymmetry of TET/TDG-dependent active DNA demethylation. (**a**) The average 5fC/5caC level on the called cytosines (n = 454,400, identified in WG-MAB-seq; FDR = 5%; sequencing depth on both strands ≥10) is significantly higher than that of cytosines on the opposite strand. Called, cytosines enriched for 5fC/5caC in *shTdg*+VC; opposite, cytosines on the opposite strand. (**b**) Distribution of differences of WG-MAB-seq signals (in *shTdg*+Vc) between called and opposite cytosines. Symmetric, both strands are called for enriching 5fC/5caC in *shTdg*+VC; asymmetric, only one strand is called. (**c**) Two-dimensional density plot of WG-MAB-seq signals at each called/opposite CpG dyad reveals the strand asymmetry of TET/TDG-dependent active DNA demethylation. (**d**) Locus-specific MAB-seq analysis of two representative loci illustrating the asymmetric distribution of 5fC/5caC. 5fC/5caC levels for the Watson strand are in blue, whereas those for the Crick strand are in red. (**e**) Bar graph of relative percentage of CpG dyads (n = 15, analyzed by locus-specific MAB-seq) that are associated with different degrees of strand asymmetry of active DNA demethylation activity in *shCtrl*, *shCtrl*+VC, *shTdg*, *shTdg*+VC mouse ESCs.

(from 41.3% to 77.7%) between 5hmC-enriched regions and 5fC/5caC peaks (pairs #3–5 in **Supplementary Fig. 9b**), probably due to their lower resolution.

Given that 5fC/5caC are preferentially enriched at active and/or poised gene regulatory regions where chromatin is generally more accessible, we reasoned that local chromatin structure may influence the occupancy level and/or processivity (the ability to further oxidize 5hmC to 5fC/5caC) of TET enzymes. We first analyzed DNase I hypersensitivity (measured by DNase-seq[30]) at genomic regions (±50 bp) immediately flanking 5fC/5caC-alone, 5hmC-alone and dual modified CpGs. This analysis reveals that 5fC/5caC-alone and dual-modified CpGs are associated with markedly higher level of DNase I hypersensitivity signals than 5hmC-alone CpGs (**Fig. 3b** and **Supplementary Fig. 9c,d**). Further analysis indicates that as compared to 5hmC-alone CpGs, 5fC/5caC-alone and dual-modified CpGs are associated with higher levels of benzonase (BNase) sensitivity signals[31], histone variants (H2A.Z and H3.3) known to destabilize nucleosome structure[31,32], TET1 occupancy[33] and pluripotency-related transcription factors (TFs; Oct4, Nanog and Sox2)[34] (**Fig. 3c**). In contrast, comparable levels of general histone H3 were detected at distinct groups of CpGs (**Fig. 3c**). These results suggest that TET proteins by default tend to stall at the 5hmC step at most CpGs, but exhibit higher processivity at CpGs associated with a more accessible chromatin state.

Strand asymmetry of 5fC/5caC in palindromic CpGs

Although cytosine methylation in palindromic CpG dyads is generally symmetric and exhibits very high heritability upon DNA replication[2], previous studies suggest that >80% of steady-state 5hmC in human and mouse ESCs are asymmetrically modified[23]. This prompted us to examine whether 5fC/5caC-modified CpGs also show strand biases (**Fig. 4a**). Focusing on CpG dyads with both strands sufficiently covered by WG-MAB-seq (n = 9,261,306 CpG dyads and depth ≥ 10 on both Watson and Crick strands), we found that only 4.97% of called CpG dyads (22,590 out of 454,400 called CpG dyads, FDR = 5%) are symmetrically modified with 5fC/5caC. Further analysis focusing on

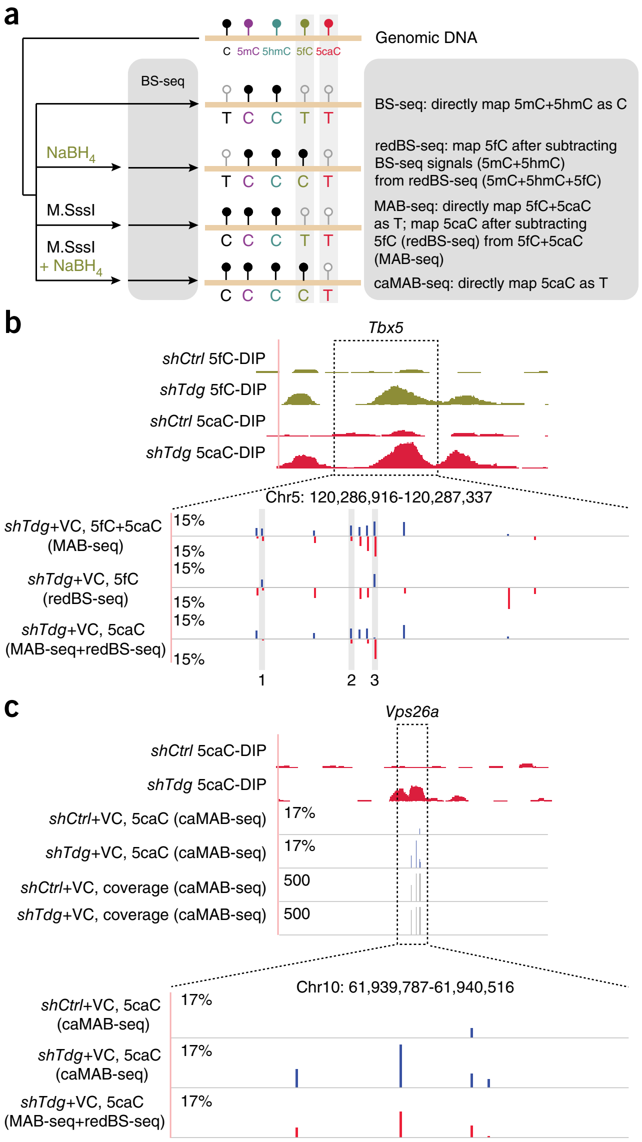

Figure 5 Base-resolution mapping analysis reveals distinct distribution patterns of 5fC and 5caC. (**a**) Schematic diagram of combining BS-seq, redBS-seq, MAB-seq and caMAB-seq to map 5fC and 5caC individually at single-base resolution. (**b**) Locus-specific analysis of 5fC and 5caC at the *Tbx5* locus indicates that 5fC and 5caC are largely nonoverlapping, and both modifications exhibit strong strand asymmetry. For comparison, affinity-based 5fC and 5caC maps are shown on the top. In enlarged views, base-resolution maps of 5fC+5caC (measured by MAB-seq), 5fC (measured by redBS-seq) and 5caC (subtraction between MAB-seq and redBS-seq) are shown. Signals for the Watson strand are in blue, whereas those for the Crick strand are in red. (**c**) Comparative locus-specific analysis of 5caC at the *Vps26a* locus by two base-resolution methods: indirect mapping through subtraction between MAB-seq and redBS-seq (red), direct mapping by caMAB-seq (blue). For comparison, also shown are DIP-seq based maps of 5caC in control and *Tdg*-depleted mouse ESCs. The level of 5caC (only Watson strand shown) is displayed as the percentage of total C modified as 5caC. Corresponding caMAB-seq sequencing depth (vertical axis limits are 0 to 500) at each CpG was also shown.

CpG dyads with both strands covered by higher sequencing depth (≥20) reached a similar conclusion (7.92% symmetrically modified with 5fC/5caC). However, because the abundance of 5fC/5caC is low at any given CpG dyad, it is still possible that sequencing depth in WG-MAB-seq might not be sufficient to identify all 5fC/5caC, leading to an underestimation of symmetrically modified CpGs. To address this issue, we pooled MAB-seq signals of all called 5fC/5caC-modified CpGs and compared the called strand to the opposite strand. The average abundance of 5fC/5caC at the called CpGs is 26.9%, whereas that of the opposite CpGs is only 8.5% (**Fig. 4a**). To further confirm the observed strand asymmetry of 5fC/5caC-modified CpG dyads, we analyzed the difference in 5fC/5caC levels of called and opposite strands for each called CpG dyads (FDR = 5%, depth ≥10). For asymmetrically modified CpGs, the difference in 5fC/5caC levels between called and opposite cytosines is on average 18.6% at each CpG dyad (or 14.4% for CpG dyads with depth ≥20) (**Fig. 4b**). Visualizing the absolute levels of 5fC/5caC on both called and opposite strands in a two-dimensional histogram plot showed a clear shift toward the called cytosines (**Fig. 4c**). Notably, similar analysis of H3K4me1-MAB-seq data sets also supports the observed strand asymmetry of 5fC/5caC-modified CpG dyads (**Supplementary Fig. 7d**–**f**). Further analysis showed no strand bias for M.SssI in methylating the lambda phage genome (97.97% for Watson strand versus 97.90% for Crick strand) or genomic DNA of *Dnmt1/3a/3b*$^{-/-}$ cells (97.82% for Watson strand and 97.80% for Crick strand). Consistent with genome-scale MAB-seq analysis, strand-specific analysis of *Tbx5* and *Vps26a* loci also revealed that the majority of 5fC/5caC-modified CpG dyads exhibit strand asymmetry (asymmetric (blue) + partially asymmetric (yellow): 86.7% in *shTdg* and 60% in *shTdg* + VC) (**Fig. 4d**,**e**). Locus-specific MAB-seq analysis of biological replicates suggests that the strand-specific distribution of 5fC/5caC detected at each CpG sites is not entirely stochastic (**Supplementary Fig. 5b**), suggesting that strand-specific 5fC/5caC generation and excision at individual CpGs is a regulated process.

Base-resolution mapping of 5fC and 5caC separately

Base-resolution mapping of 5fC has recently been demonstrated using subtraction-based, chemical modification–assisted BS-seq methods such as fCAB-seq[19] and redBS-seq[21] (**Supplementary Fig. 1a**). However, the relatively low protection rate of 5caC deamination (50–60%) reported in a similar subtraction-based 5caC mapping approach (caCAB-seq) suggests that further optimization is required[20]. To achieve 5caC mapping at base-resolution, we combined MAB-seq with the 5fC mapping method, redBS-seq[21] (**Fig. 5a**). After validating redBS-seq using synthetic oligonucleotides (**Supplementary Fig. 10a**), we performed locus-specific redBS-seq and BS-seq to quantify 5fC at 73 CpG sites from four loci enriched for 5fC and/or 5caC (*Tbx5*, *Vps26a*, *Slc2a12* and *Ace*). The abundance and position of 5caC at these sites can then be determined by subtracting 5fC signals (derived from the difference between redBS-seq and BS-seq) from the levels of 5fC+5caC measured by MAB-seq (**Fig. 5b** and **Supplementary Fig. 10c**,**d**). Using this integrative approach to map 5fC and 5caC separately, we observed that 5fC and 5caC displayed largely distinct distribution patterns at individual CpGs within these loci. For instance, within exon2 of *Tbx5*, a region enriched for both 5fC and 5caC, some CpG sites were only modified with 5fC (CpG #1 at *Tbx5* in **Fig. 5b**), whereas some others were 5caC-only (CpG #2 at *Tbx5* in **Fig. 5b**). More strikingly, as exemplified by CpG #3 at *Tbx5* in **Figure 5b**, CpG sites associated with both 5fC and 5caC may exhibit nonoverlapping, strand-specific 5fC/5caC distribution. This conclusion is further supported by analysis of an active enhancer within the *Vps26a* gene (**Supplementary Fig. 10d**). Such diverse distribution patterns of 5fC and 5caC indicate the distinct processivity of TETs and/or substrate preference of TDG (5fC versus 5caC) at individual CpGs. Notably, most 5fC-modified CpGs (20 out of 24) identified by redBS-seq were also detected by MAB-seq as 5fC/5caC-modified (**Supplementary Fig. 10c**). The few inconsistent sites between MAB-seq and redBS-seq probably arise from the different principles that the two methods are based upon.

Base-resolution mapping 5caC through integrating MAB-seq and redBS-seq requires two rounds of subtractions, representing a technical challenge for genome-scale analysis. Thus, we explored a subtraction-independent 5caC mapping strategy by taking advantage of the fact that 5fC can be selectively reduced by sodium borohydride ($NaBH_4$) to 5hmC[19,21]. In this modified version of MAB-seq (termed caMAB-seq), M.SssI-treated DNA was further incubated with $NaBH_4$ so that only 5caC was read as T in bisulfite sequencing (**Fig. 5a**). Analyses of defined sequences (lambda DNA or synthetic oligonucleotides) or 5caC-enriched genomic loci (e.g., *Vps26a*) demonstrated the validity of caMAB-seq in direct base-resolution mapping of 5caC (**Fig. 5c** and **Supplementary Fig. 10b**,**e**).

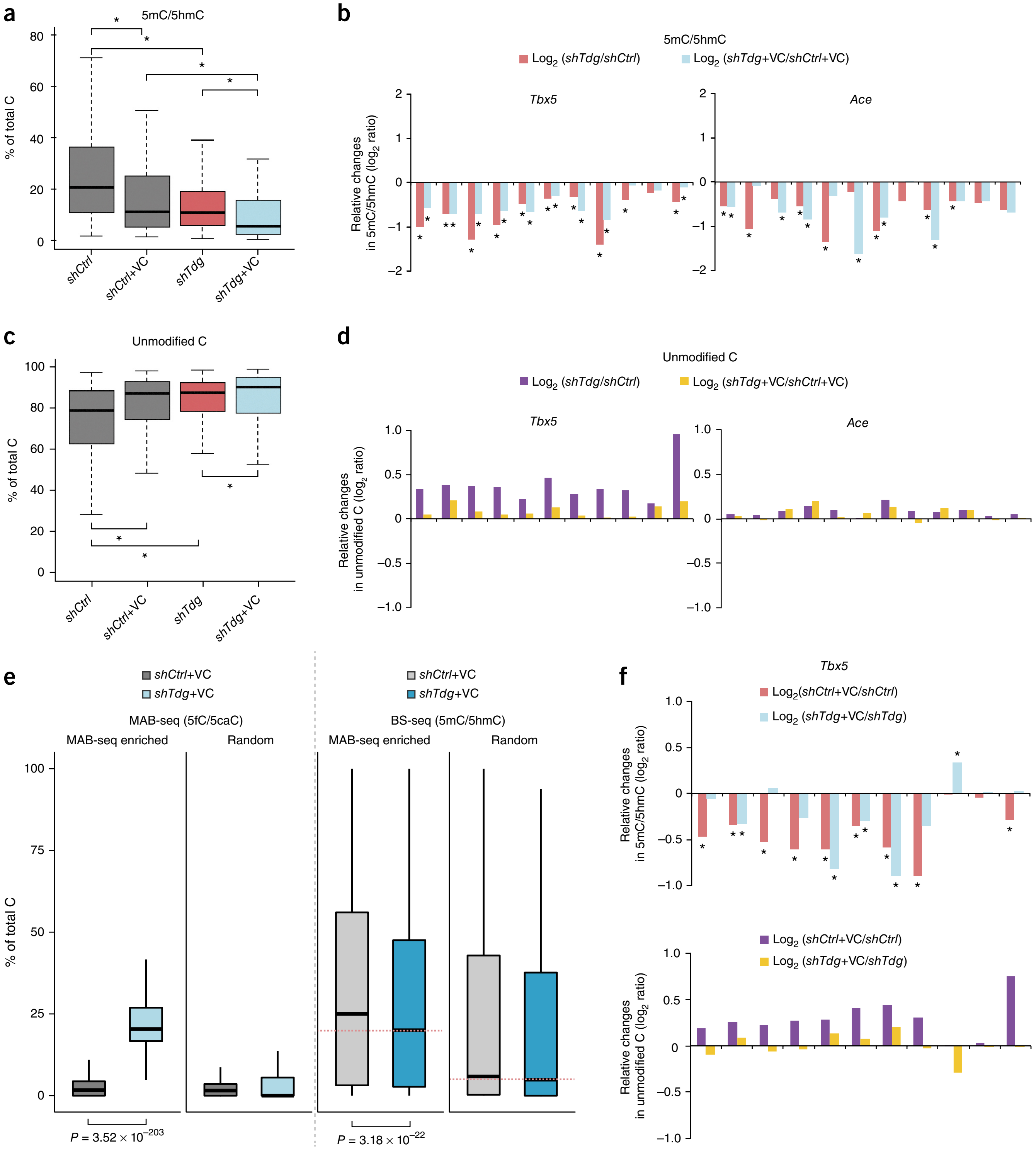

Integrative analysis of unmodified C, 5mC/5hmC and 5fC/5caC

Standard BS-seq cannot distinguish unmodified C from 5fC/5caC. When combined with BS-seq, MAB-seq was able to quantify the true abundance of unmodified CpG at base-resolution (**Fig. 1a**), providing a unique opportunity for exploring the potential role of 5fC/5caC excision in regulating upstream (5mC + 5hmC) and downstream (unmodified C) steps in the TET/TDG-dependent active DNA demethylation pathway. By performing locus-specific BS-seq and MAB-seq through Illumina deep sequencing, we quantified the levels of unmodified C, 5mC/5hmC and 5fC/5caC at 73 CpGs within four 5fC/5caC-enriched regions. BS-seq analysis showed that *Tdg*-depletion induced a significant decrease in 5mC/5hmC within these loci (*shTdg* versus *shCtrl* or *shTdg*+VC versus *shCtrl*+VC in **Fig. 6a**). Further analysis shows that significant decrease in 5mC/5hmC was detected at multiple CpGs within each locus (**Fig. 6a**,**b** and **Supplementary Fig. 11a**). In contrast to 5mC/5hmC, integrative analysis of BS-seq and MAB-seq results revealed that unmodified C was significantly increased in response to TDG depletion (**Fig. 6c**,**d** and **Supplementary Fig. 11b**).

Tdg-depletion induced changes in 5mC/5hmC and unmodified C appeared to be more pronounced at *Tbx5*, *Ace* and *Slc2a12* loci when compared to *Vps26a* locus (an active enhancer), suggesting that active DNA demethylation dynamics at these transcriptionally repressed and/or poised regions (previously determined by ChIP-seq) was modulated by the generation and/or excision of 5fC/5caC. To test this possibility at a genome-scale, we captured genomic regions marked by H3K27me3, a repressive histone modification associated with transcriptionally poised gene promoters of lineage-specific TFs (e.g., *Tbx5*), and subjected H3K27me3-enriched DNA to genome-scale MAB-seq and BS-seq analyses. H3K27me3-MAB-seq identified 1,231 genomic intervals enriched for 5fC/5caC signals in *shTdg*+VC cells, and H3K27me3-BS-seq showed that there was a significant decrease in 5mC/5hmC levels within these 5fC/5caC-enriched regions ($P = 3.18 \times 10^{-22}$, Wilcoxon) ("MAB-seq enriched" in **Fig. 6e**). For 1,231 randomly sampled regions where 5fC/5caC signals are largely absent, the change in 5mC/5hmC is much less pronounced ("random" in **Fig. 6e**). Consistent with results of locus-specific analysis, genome-scale analysis supports the notion that inhibition of TDG-mediated 5fC/5caC excision may lead to dysregulation of upstream steps of the cytosine-modifying cascade.

Notably, VC treatment alone substantially reduced the level of 5mC/5hmC (*shCtrl*+VC versus *shCtrl* or *shTdg*+VC versus *shTdg* in **Figure 6a** and upper panels in **Fig. 6f**), possibly due to its positive effect on stimulating TET catalytic activity (oxidizing 5mC/5hmC). In addition, VC treatment induced a significant increase in the level of unmodified C (*shCtrl*+VC versus *shCtrl* or *shTdg*+VC versus *shTdg* in **Fig. 6c**). However, the VC-induced increase in unmodified C was more pronounced in *shCtrl* (purple in lower panel of **Fig. 6f**) than in *shTdg* (yellow in lower panel of **Fig. 6f**), indicating that accumulation of unmodified C by VC treatment required a TDG/BER-mediated 5fC/5caC excision step. Together, these results suggest that inhibition of 5fC/5caC excision step by depleting TDG proteins or accumulation of 5fC/5caC itself may result in dysregulation of both upstream (5mC/5hmC generation or oxidization) and downstream (generation and/or methylation of unmodified C) steps of the DNMT/TET/TDG-dependent cytosine-modifying cascade.

DISCUSSION

In this study, we have established an approach, MAB-seq, for quantitative measurement of 5fC/5caC excision repair-dependent active DNA demethylation activity at base-resolution, providing a tool that has broad application in the study of active DNA demethylation. A major advantage of MAB-seq over other subtraction-based 5fC or 5caC mapping methods is the ability to directly determine the location and abundance of 5fC and 5caC in a single experiment. MAB-seq can therefore achieve similar sensitivity for detecting 5fC/5caC with lower sequencing depth and simplifies the computational procedure to confidently identify CpGs marked 5fC/5caC. When combined with *Tdg* depletion, simultaneous mapping 5fC and 5caC enables quantitative measurement of the generation and excision of 5fC/5caC, providing a direct readout of the TET/TDG-mediated active DNA demethylation activity.

Application of WG MAB-seq analysis to mouse ESCs allowed us to investigate the genomic architecture and dynamics of active DNA demethylation activity at single-base resolution across the genome of this stem cell population. Although affinity-based 5fC and 5caC mapping methods suggest that 5hmC- and 5fC/5caC-enriched regions largely overlap[18,19], comparative analysis of base-resolution 5fC/5caC map and 5hmC map reveals that a large fraction of 5fC/5caC and 5hmC are associated with distinct CpGs within 5hmC/5fC/5caC-enriched regions. Additional analyses support a model in which TET proteins tend to stall at the 5hmC step at most CpGs, but exhibit higher processivity to further oxidize 5hmC to 5fC/5caC at CpGs with higher chromatin accessibility. Moreover, integrating MAB-seq with 5fC-mapping (e.g., redBS-seq) or 5caC-mapping (e.g., caMAB-seq) method not only provides a base-resolution approach to map 5fC and 5caC separately, but also reveals that 5fC and 5caC frequently do not overlap at individual CpGs. These findings suggest the possibility that TET exhibits distinct processivity depending on local chromatin accessibility or other yet-to-be-identified regulatory processes. It is also possible that TDG may

Figure 6 Base-resolution mapping of unmodified C and 5mC/5hmC reveals that TDG-mediated 5fC/5caC excision affects active demethylation dynamics. (**a**) *Tdg* knockdown and/or VC treatment results in a significant decrease in BS-seq signals (5mC+5hmC). Shown are boxplots summarizing the levels of 5hmC+5mC at 73 CpG sites from *Ace*, *Slc2a12*, *Tbx5* and *Vps26a* loci. An asterisk indicates a statistically significant difference between the two indicated groups, as determined by Wilcoxon signed-rank test for matched pairs (multiple comparison corrected $P < 0.05$). (**b**) Shown are relative changes in 5mC+5hmC levels ($\log_2$ ratio) in response to *Tdg* knockdown at individual CpG sites from *Ace* and *Tbx5* loci. *shTdg* was compared with *shCtrl* while *shTdg*+VC was compared with *shCtrl*+VC. An asterisk indicates a statistically significant change determined by Fisher's exact test (multiple comparison corrected $P < 0.05$). (**c**) *Tdg* knockdown or VC treatment leads to a significant increase in the level of unmodified C (measured by subtracting C signals in BS-seq from those of MAB-seq). Shown are boxplots summarizing the levels of unmodified C at 73 CpG sites from *Ace*, *Slc2a12*, *Tbx5* and *Vps26a* loci. An asterisk indicates a statistically significant difference between the two indicated groups (multiple comparison corrected $P < 0.05$, Wilcoxon signed-rank test for matched pairs). (**d**) Shown are relative changes in unmodified C levels ($\log_2$ ratio) in response to *Tdg* knockdown at individual CpG sites from *Ace* and *Tbx5* loci. *shTdg* was compared with *shCtrl* while *shTdg*+VC was compared with *shCtrl*+VC. (**e**) Genome-scale H3K27me3-MAB-seq and H3K27me3-BS-seq analyses in control or *Tdg*-depleted mouse ESCs show that 5m/5hmC levels are significantly decreased within genomic regions enriched for 5fC/5caC. Boxplots depicting MAB-seq and BS-seq signals (binned to 500-bp intervals) are shown for 5fC/5caC-enriched regions. Equal number of randomly sampled regions that are covered by both BS-seq and MAB-seq are analyzed. (**f**) Relative changes ($\log_2$ ratio) in 5mC+5hmC levels (top panels) and unmodified C levels (bottom panels) in response to VC treatment. *shCtrl*+VC was compared with *shCtrl* while *shTdg*+VC was compared with *shTdg*. For relative changes in 5mC+5hmC levels, an asterisk indicates a statistically significant change determined by Fisher's exact test (multiple comparison corrected $P < 0.05$).

exhibit distinct activity or substrate preference at different CpGs. In addition, simultaneous mapping of 5fC/5caC by MAB-seq reveals that TET/TDG-dependent active DNA demethylation activity preferentially targets palindromic CpG dyads asymmetrically, supporting the recently proposed asymmetric base-flipping model[24,25]. Lastly, we demonstrate that integrative analysis of MAB-seq and BS-seq data sets allows quantitative measurement of cytosine derivatives at all major steps of the TET/TDG-mediated active demethylation pathway (iterative oxidation (5mC/5hmC), excision repair (5fC/5caC) and regeneration (unmodified C)), and reveals that 5fC/5caC excision by TDG may act as a regulatory checkpoint of the active DNA demethylation cascade.

In addition to a robust base-resolution mapping method for 5fC/5caC, we provide here a WG base-resolution map of TET/TDG-dependent active DNA demethylation activity in the mammalian genome. Given the simplicity and cost effectiveness of MAB-seq, we anticipate that genome-scale MAB-seq analysis can be applied to analyze diverse cell types in future studies to provide new insights into the mechanism and function of the DNMT-TET-TDG/BER cytosine-modifying cascade. Thus, the 5fC/5caC mapping technology described in this study and other base-resolution mapping methods[19,21,23,35] set the stage for systematic investigation of the functional significance of active DNA demethylation in mammalian development and human diseases.

METHODS

Methods and any associated references are available in the online version of the paper.

Accession codes. GEO: GSE62631

Note: Any Supplementary Information and Source Data files are available in the online version of the paper.

ACKNOWLEDGMENTS

We thank S. Yamaguchi and F. Lu for generating and characterizing Tet mutant mouse ESCs. We also thank L.M. Tuesta and S. Yamaguchi for critical reading of the manuscript. This project is supported by National Institutes of Health grant U01DK089565. H.W. was supported by a postdoctoral fellowship from the Jane Coffin Childs Memorial Fund for Medical Research and is currently supported by the National Human Genome Research Institute (K99HG007982). X.W. was supported by the China Scholarship Council. Y.Z. is an investigator of the Howard Hughes Medical Institute.

AUTHOR CONTRIBUTIONS

H.W. and Y.Z. conceived the project. H.W. and X.W. performed experiments and carried out data analysis. L.S. performed sequencing. H.W., X.W. and Y.Z. wrote the manuscript.

COMPETING FINANCIAL INTERESTS

The authors declare no competing financial interests.

Reprints and permissions information is available online at http://www.nature.com/reprints/index.html.

1. Bestor, T.H. The DNA methyltransferases of mammals. *Hum. Mol. Genet.* **9**, 2395–2402 (2000).
2. Bird, A. DNA methylation patterns and epigenetic memory. *Genes Dev.* **16**, 6–21 (2002).
3. Cedar, H. & Bergman, Y. Programming of DNA methylation patterns. *Annu. Rev. Biochem.* **81**, 97–117 (2012).
4. Baylin, S.B. & Jones, P.A. A decade of exploring the cancer epigenome - biological and translational implications. *Nat. Rev. Cancer* **11**, 726–734 (2011).
5. Wu, H. & Zhang, Y. Reversing DNA methylation: mechanisms, genomics, and biological functions. *Cell* **156**, 45–68 (2014).
6. Pastor, W.A., Aravind, L. & Rao, A. TETonic shift: biological roles of TET proteins in DNA demethylation and transcription. *Nat. Rev. Mol. Cell Biol.* **14**, 341–356 (2013).
7. Tahiliani, M. *et al.* Conversion of 5-methylcytosine to 5-hydroxymethylcytosine in mammalian DNA by MLL partner TET1. *Science* **324**, 930–935 (2009).
8. Ito, S. *et al.* Role of Tet proteins in 5mC to 5hmC conversion, ES-cell self-renewal and inner cell mass specification. *Nature* **466**, 1129–1133 (2010).
9. Ito, S. *et al.* Tet proteins can convert 5-methylcytosine to 5-formylcytosine and 5-carboxylcytosine. *Science* **333**, 1300–1303 (2011).
10. He, Y.F. *et al.* Tet-mediated formation of 5-carboxylcytosine and its excision by TDG in mammalian DNA. *Science* **333**, 1303–1307 (2011).
11. Inoue, A. & Zhang, Y. Replication-dependent loss of 5-hydroxymethylcytosine in mouse preimplantation embryos. *Science* **334**, 194 (2011).
12. Maiti, A. & Drohat, A.C. Thymine DNA glycosylase can rapidly excise 5-formylcytosine and 5-carboxylcytosine: potential implications for active demethylation of CpG Sites. *J. Biol. Chem.* **286**, 35334–35338 (2011).
13. Nabel, C.S. *et al.* AID/APOBEC deaminases disfavor modified cytosines implicated in DNA demethylation. *Nat. Chem. Biol.* **8**, 751–758 (2012).
14. Cortázar, D. *et al.* Embryonic lethal phenotype reveals a function of TDG in maintaining epigenetic stability. *Nature* **470**, 419–423 (2011).
15. Cortellino, S. *et al.* Thymine DNA glycosylase is essential for active DNA demethylation by linked deamination-base excision repair. *Cell* **146**, 67–79 (2011).
16. Kriaucionis, S. & Heintz, N. The nuclear DNA base 5-hydroxymethylcytosine is present in Purkinje neurons and the brain. *Science* **324**, 929–930 (2009).
17. Lister, R. *et al.* Global epigenomic reconfiguration during Mammalian brain development. *Science* **341**, 1237905 (2013).
18. Shen, L. *et al.* Genome-wide analysis reveals TET- and TDG-dependent 5-methylcytosine oxidation dynamics. *Cell* **153**, 692–706 (2013).
19. Song, C.-X. *et al.* Genome-wide profiling of 5-formylcytosine reveals its roles in epigenetic priming. *Cell* **153**, 678–691 (2013).
20. Lu, X. *et al.* Chemical modification-assisted bisulfite sequencing (CAB-Seq) for 5-carboxylcytosine detection in DNA. *J. Am. Chem. Soc.* **135**, 9315–9317 (2013).
21. Booth, M.J., Marsico, G., Bachman, M., Beraldi, D. & Balasubramanian, S. Quantitative sequencing of 5-formylcytosine in DNA at single-base resolution. *Nat. Chem.* **6**, 435–440 (2014).
22. Renbaum, P. *et al.* Cloning, characterization, and expression in *Escherichia coli* of the gene coding for the CpG DNA methylase from *Spiroplasma* sp. strain MQ1 (M.SssI). *Nucleic Acids Res.* **18**, 1145–1152 (1990).
23. Yu, M. *et al.* Base-resolution analysis of 5-hydroxymethylcytosine in the mammalian genome. *Cell* **149**, 1368–1380 (2012).
24. Hu, L. *et al.* Crystal Structure of TET2-DNA complex: insight into TET-mediated 5mC oxidation. *Cell* **155**, 1545–1555 (2013).
25. Hashimoto, H. *et al.* Structure of a Naegleria Tet-like dioxygenase in complex with 5-methylcytosine DNA. *Nature* **506**, 391–395 (2014).
26. Yin, R. *et al.* Ascorbic acid enhances Tet-mediated 5-methylcytosine oxidation and promotes DNA demethylation in mammals. *J. Am. Chem. Soc.* **135**, 10396–10403 (2013).
27. Blaschke, K. *et al.* Vitamin C induces Tet-dependent DNA demethylation and a blastocyst-like state in ES cells. *Nature* **500**, 222–226 (2013).
28. Mikkelsen, T.S. *et al.* Genome-wide maps of chromatin state in pluripotent and lineage-committed cells. *Nature* **448**, 553–560 (2007).
29. Sotiriou, S. *et al.* Ascorbic-acid transporter Slc23a1 is essential for vitamin C transport into the brain and for perinatal survival. *Nat. Med.* **8**, 514–517 (2002).
30. Encode Project Consortium. A user's guide to the encyclopedia of DNA elements (ENCODE). *PLoS Biol.* **9**, e1001046 (2011).
31. Hu, G. *et al.* H2A.Z facilitates access of active and repressive complexes to chromatin in embryonic stem cell self-renewal and differentiation. *Cell Stem Cell* **12**, 180–192 (2013).
32. Banaszynski, L.A. *et al.* Hira-dependent histone H3.3 deposition facilitates PRC2 recruitment at developmental loci in ES cells. *Cell* **155**, 107–120 (2013).
33. Wu, H. *et al.* Dual functions of Tet1 in transcriptional regulation in mouse embryonic stem cells. *Nature* **473**, 389–393 (2011).
34. Whyte, W.A. *et al.* Master transcription factors and mediator establish super-enhancers at key cell identity genes. *Cell* **153**, 307–319 (2013).
35. Booth, M.J. *et al.* Quantitative sequencing of 5-methylcytosine and 5-hydroxymethylcytosine at single-base resolution. *Science* **336**, 934–937 (2012).

ONLINE METHODS

Mouse ESC cultures, lentiviral knockdown of TDG and vitamin C treatment. V6.5 (control and *Tdg* knockdown), E14Tg2A (control, *Tdg* knockdown and *Tet1/2*$^{-/-}$), and J1 (*Dnmt1/3a/3b*$^{-/-}$) mouse ESC lines were cultured in feeder-free gelatin-coated plates in Dulbecco's Modified Eagle Medium (DMEM) (GIBCO, 11995) supplemented with 15% FBS (GIBCO), 2 mM L-glutamine (GIBCO), 0.1 mM 2-mercaptoethanol (Sigma), nonessential amino acids (GIBCO), 1,000 units/ml LIF (Millipore, ESG1107). The culture was passaged every 2–3 d using 0.05% Trypsin (GIBCO). Lentivirus-mediated *Tdg* knockdown in mouse ESCs were performed as previously described[18]. For vitamin C (Sigma, A8960) treatment, control and *Tdg* knockdown mouse ESCs were treated with 100 μg/ml of vitamin C for 60 h.

Chromatin immunoprecipitation for genome-scale MAB-seq/BS-seq. To capture H3K4me1- or H3K27me3-enriched chromatin for genome-scale MAB-seq analysis, 1–2 × 10^7 cells were cross-linked with 1% formaldehyde for 10 min at room temperature followed by exposure to 0.125 M glycine. After two washes with cold PBS, cells were collected and stored at −80 °C before use. Nuclei were extracted and lysed sequentially with lysis buffer 1 (LB1, 50 mM Hepe2-KOH, pH7.5, 140 mM NaCl, 1 mM EDTA, 10% glycerol, 0.5% NP40, 0.25% Triton X-100), lysis buffer 2 (LB2, 10 mM Tris-HCl, pH8.0, 200 mM NaCl, 1 mM EDTA, 0.5 mM EGTA), and lysis buffer 3 (LB3, 10 mM Tris-HCl, pH8.0, 100 mM NaCl, 1 mM EDTA, 0.5 mM EGTA, 0.1% Na-Deoxycholate, 0.5% *N*-lauroylsarcosine). Chromatin was sonicated using a microtip (Branson sonifier 450) until the DNA fragments were reduced to 200–1,000 bp in length. 10 μg antibodies were immobilized with 100 μl Dynal protein-G beads (Invitrogen) for at least 6 h. Immunoprecipitation was performed overnight at 4 °C with antibody-conjugated protein-G beads. DNA/protein complexes were washed with RIPA buffer (50 mM Hepes-KOH, pH7.6, 500 mM LiCl, 1 mM EDTA, 1% NP-40, 0.7% Na-Deoxycholate) for five times and reverse cross-linked at 65 °C overnight. The DNA was treated sequentially with RNase A and proteinase K, and purified by phenol/chloroform extraction and ethanol precipitation. The following antibodies were used in ChIP assays: anti-H3K4me1 (ab8895, Abcam 10 μg/ml) and anti-H3K27me3 (07-449, Millipore 10 μg/ml).

Library generation for genome-scale MAB-seq/BS-seq. 200–500 ng of ChIP DNA (H3K4me1-enriched or H3K27me3-enriched) was first spiked-in with unmethylated lambda DNA (1:400), which was then repaired and ligated to methylated (5mC) custom adapters (forward 5′-ACACTCTTTCCCTACACGACGCTCTTCCGATC*T-3′; reverse 5′-/5Phos/GATCGGAAGAGCACACGTCTGAACTCCAGTC-3′; the asterisk denotes phosphorothioate bond) with the NEBNext Ultra DNA Library Prep kit from Illumina (NEB). Adaptor-ligated DNA was then purified with 1.2× AMPure XP beads (Beckman Coulter). For BS-seq, methylated-adaptor-ligated DNA was directly subjected to bisulfite conversion using Qiagen EpiTect DNA Bisulfite Kit (Qiagen, 59104) per manufacturer's instructions, except that the thermal cycle was repeated twice. For MAB-seq, methylated adaptor-ligated DNA was treated by M.SssI (New England Biolabs, M0226M) in a 50-μl reaction for two rounds. In each round of treatment, DNA was first incubated with 1.0 unit/μl M.SssI methylase (New England Biolabs, M0226M) for 4 h in 25-μl reaction (1.25 μl of 20 unit/μl M.SssI and 0.5 μl of 32 mM SAM (final concentration: 640 μM)), and additional 25-μl containing same concentration of M.SssI (1.0 unit/μl) and SAM (640 μM) was supplemented to treat DNA for another 8 h (in 50 μl). Of note, the first round of M.SssI treatment was performed in Mg^{2+}-free reaction buffer (10 mM Tris-HCl (pH 8.0), 50 mM NaCl, 10 mM EDTA), whereas the second round was carried out with NEB buffer #2 (10 mM Tris-HCl (pH 7.9), 50 mM NaCl, 10 mM $MgCl_2$, 1 mM DTT). DNA was purified by sequential phenol/chloroform/isoamyl alcohol (PCI, 25:24:1) extraction and ethanol precipitation after each round of M.SssI treatment. M.SssI-treated, methylated adaptor-ligated DNA was then subjected to bisulfite conversion using the EpiTect DNA Bisulfite Kit (Qiagen) as described above. Bisulfite-treated DNA was pre-amplified for 5 cycles using KAPA HiFi Uracil$^+$ HotStart ReadyMix (Kapa Biosystems, KK2801) with indexed and universal primers from NEBNext Multiplex Oligos for Illumina (Index Primers Set 1). The optimal PCR cycle numbers required to generate the final libraries were then determined by quantitative PCR. Final libraries were generated by scaled-up PCR reactions using the cycles determined above, and purified with 1.2× AMPure XP beads. For whole genome (WG) MAB-seq analysis, genomic DNA was extracted from mESCs using the DNeasy Blood & Tissue Kit (Qiagen 69504). 1 μg nonenriched genomic DNA was first spiked-in with unmethylated lambda DNA (1:400) and was then treated with M.SssI (1st round protocol). M.SssI-treated genomic DNA (in 50-μl) was fragmented to an average size of 300–400 bp with Covaris M220 (20% duty factor, 200 cycles per burst, 80 s × 2). Sheared DNA was purified (1.2× AMPure XP beads), end-repaired and ligated to methylated adapters as described for H3K4me1/H3K27me3-MAB-seq. Methylated-adapter-ligated DNA was treated with M.SssI again (2nd round protocol) before bisulfite conversion (Qiagen EpiTect DNA Bisulfite Kit). Bisulfite-treated DNA was prepared for sequencing as described above.

Data processing of genome-scale MAB-seq/BS-seq. Raw sequencing reads were trimmed for low-quality bases and adaptor sequences using Trimmomatic[36], and the data quality was examined with FastQC (http://www.bioinformatics.babraham.ac.uk/projects/fastqc/). The trimmed reads were mapped against the mouse genome (mm9 build) with Bismark[37]. PCR duplicates were removed using the Picard program (http://picard.sourceforge.net/). Cell line-specific SNPs overlapping with CpGs in the mouse genome (mm9) were filtered out with BisSNP[38]. All programs were performed with default setting. For MAB-seq analysis, raw signals were calculated as % of T/(C+T) at each called CpG. For BS-seq analysis, raw signals were calculated as % of C/(C+T) at each called CpG. Statistics of all genome-scale sequencing libraries is summarized in **Supplementary Table 1**.

Statistical calling of 5fC/5caC and assessing FDR of genome-scale MAB-seq. For each cytosine within CpG dinucleotides, we counted the number of "T" bases from MAB-seq reads as 5fC/5caC (denoted N_T) and the number of "C" bases as other forms of cytosines (C/5mC/5hmC; denoted N_C). Next, we used the binomial distribution (N as the sequencing coverage ($N_T + N_C$) and p as the error rate (2.04%) of M.SssI methylase) to assess the probability of observing N_T or greater by chance. To estimate empirical FDR of calling 5fC/5caC-modified CpGs, we repeated the steps above on MAB-seq signals of merged negative control sample (*Dnmt1/3a/3b*$^{-/-}$ and *Tet1/2*$^{-/-}$) in which 5fC/5caC is largely absent. The FDR for a given *P*-value cutoff of the binomial distribution is the number of called CpGs in negative controls divided by the number detected in the sample of *Tdg*-deficient VC-treated mouse ESCs. For calling 5fC/5caC-modified CpG dyads (**Fig. 2c**), reads covering Watson strand and Crick strand of the same CpG dyads were combined, and we restricted our analysis to CpG dyads covered by at least five reads. For **Figures 3** and **4**, strand-specific analysis was performed and we restricted our analysis to CpGs covered by at least ten reads.

Validation of MAB-seq by synthetic 38-bp oligonucleotides. To monitor the behavior of C and modified C in MAB-seq, 38-bp single-stranded DNA oligos were synthesized (forward strand: 5′-AGCC**XGXG**C**XGXG**C**XG**GT**XG**AG**XG**GC**XG**CTCC**XG**CAGC-3′, reverse (complementary) strand: 5′-GCTG**XG**GGAG**XG**GC**XG**CT**XG**AC**XG**G**XGXG**G**XGXG**GGCT-3′, in which X is either unmodified C, 5hmC, 5fC or 5caC). To test whether M.SssI treatment alters the behavior of 5hmC, 5fC and 5caC during bisulfite sequencing, forward strands containing 5hmC, 5fC and 5caC were annealed to reverse strands containing the same modified Cs and ligated to methylated adaptors. The resulting oligos were treated by M.SssI using the same protocol used for locus-specific MAB-seq (described below), followed by bisulfite conversion and deep sequencing to determine their behavior. To test whether M.SssI functions at hemi-5hmC, 5fC and 5caC CpGs, top strands containing 5hmC, 5fC and 5caC were annealed to bottom strand containing unmodified C. The same experimental procedures were undertaken to assess the efficiency of M.SssI in these contexts.

Locus-specific MAB-seq of genomic DNA. 1 μg genomic DNA was treated by M.SssI in a 50 μl reaction for four rounds. During each round of treatment, DNA was first treated by M.SssI for 2 h (1.5 μl M.SssI and 1 μl SAM), and additional M.SssI and SAM were supplemented to treat DNA for another 4 h (0.5 μl M.SssI, 1 μl SAM), increasing the total concentration of the enzyme to 0.8 unit/μl. DNA was purified by PCI after each round of treatment.

doi:10.1038/nbt.3073

After M.SssI treatment, bisulfite conversion was performed as described above. Selected loci were amplified by PCR using KAPA HiFi Hotstart Uracil+ DNA polymerase followed by sonication by Bioruptor (Diagenode), library preparation using NEBNext DNA Library Prep Master Mix Set (New England Biolabs) and deep sequencing by Illumina HiSeq 2500 sequencer. Alternatively, PCR-amplified DNA was cloned into TOPO vectors (Zero Blunt TOPO Cloning Kit, Invitrogen) for standard Sanger sequencing. Primer sequences for all locus-specific MAB-seq experiments were summarized in **Supplementary Table 2**.

5fC/5caC calling for locus-specific MAB-seq. In a MAB-seq experiment, 5fC and 5caC are read as T while unmodified C, 5mC and 5hmC are read as C. For a CpG site, if we name the number of T reads as N_T and the number of C reads as N_C, 5fC+5caC level (MAB-seq raw signal before background subtraction) can be calculated as $N_T/(N_T+N_C)$. Because conversion of unmodified C to 5mC by M.SssI cannot reach 100%, some T reads may come from incomplete methylation rather than real 5fC/5caC, leading to an overestimation of 5fC/5caC level. To estimate the level of these background signals resulted from incomplete conversion, $Tet1/2^{-/-}$ mouse ESCs was examined by MAB-seq, and any 5fC/5caC signal detected in this negative control is treated as background signal (false positive).

To call 5fC/5caC-positive CpG sites in a locus-specific MAB-seq experiment, MAB-seq signals detected in *shCtrl, shCtrl*+VC, *shTdg* and *shTdg*+VC samples were compared to the background signals detected in $Tet1/2^{-/-}$ sample. For a CpG site in a tested sample, Fisher's exact test was performed using N_C and N_T of the tested sample and $Tet1/2^{-/-}$ sample to determine whether MAB-seq signal at this CpG site is significantly different from the corresponding background signal. False-discovery rate (FDR) control based on Benjamini–Hochberg procedure was then performed to correct the p values for multiple comparisons, and $P < 0.05$ was used as a cut-off value to generate a list of CpG sites of which MAB-seq signals are significantly different from the background signals detected in $Tet1/2^{-/-}$ sample. After that, we further applied the numeric filter that real 5fC/5caC signals should be numerically higher than background signals, generating the list of CpG sites that are 5fC/5caC positive.

Calculating 5fC/5caC level in locus-specific MAB-seq. In $Tet1/2^{-/-}$ sample, certain background (false-positive) signals were indeed detected by MAB-seq. These background signals were subtracted from raw MAB-seq signals when calculating real 5fC/5caC levels. For example, if raw MAB-seq signal detected at a CpG site in our sample of interest is a% while the corresponding background signal detected in $Tet1/2^{-/-}$ sample is b%, and if a ≥ b, then (a – b)% will be the 5fC/5caC level. If a < b is observed (in some rare cases), then 5fC/5caC level at that CpG site in our sample of interest will be set as 0%. To determine whether the 5fC/5caC level at a group of CpG sites in one sample is different from that in another sample, Wilcoxon signed-rank test for matched pairs was performed.

Analysis of strand asymmetry of 5fC/5caC in locus-specific MAB-seq. For **Figures 4d**,**e**, 11 palindromic CpG dyads from *Tbx5* locus and 4 palindromic CpG dyads from *Vps26a* locus were examined by locus-specific MAB-seq to determine whether strand asymmetry of 5fC/5caC exists. 5fC/5caC calling was achieved through performing Fisher's exact test, and the 15 CpG dyads were first categorized into three groups: no significant 5fC/5caC signal on either the top or bottom strands; significant 5fC/5caC signal on one strand but not the other; significant 5fC/5caC signals on both strands. The existence of the second group is a direct support for strand asymmetry of 5fC/5caC. As for the third group of CpG dyads, Fisher's exact test was performed to determine whether 5fC/5caC levels differ significantly between the top and bottom strands, and this group was further separated into two groups. For each CpG dyad, if 5fC/5caC levels differ significantly between strands, this CpG dyad is categorized as "partially asymmetric" in (**Fig. 4e**).

Data analysis of locus-specific BS-seq. In BS-seq experiment, unmodified C, 5fC and 5caC are read as T while 5mC and 5hmC are read as C. For a CpG site, if we name the number of T reads as N_T and the number of C reads as N_C, 5mC + 5hmC level at this CpG site (before background subtraction) will be calculated as $N_C/(N_T + N_C)$. To determine whether the 5mC+5hmC level at a CpG site is altered by *Tdg* knockdown or vitamin C treatment, Fisher's exact test was performed. To determine whether the 5mC + 5hmC level at a group of CpG sites in one sample is different from that in another sample, Wilcoxon signed-rank test for matched pairs was performed.

Calculating the level of unmodified cytosines by combining locus-specific MAB-seq with BS-seq. For each CpG site, the true level of 5fC + 5caC was calculated by subtracting the background signal from the raw MAB-seq signal as described above. The level of 5hmC + 5mC was measured by BS-seq. The level of unmodified C equals to 100% – (abundance of 5fC+5caC) – (abundance of 5hmC + 5mC). To determine whether the unmodified C level at a group of CpG sites in one sample is different from that in another sample, Wilcoxon signed-rank test for matched pairs was performed.

Locus-specific redBS-seq of genomic DNA. redBS-seq was performed as previously described[21]. In short, 5 µl freshly made sodium borohydride aqueous solution (1M) was added to 250 ng DNA diluted in 15 µl water. The reaction was placed in darkness for an hour, quenched by 10 µl sodium acetate (0.75 M, pH = 5) and purified by PCI extraction. Bisulfite conversion was then performed as described above, followed by PCR amplification of specific loci and deep sequencing analysis of PCR amplicons.

Analysis of locus-specific redBS-seq data. In a redBS-seq experiment, 5mC, 5hmC and 5fC are read as C whereas unmodified C and 5caC are read as T. For a CpG site, the difference between the levels of C signal measured by redBS-seq and BS-seq was calculated to represent the level of 5fC. In rare cases when negative values were obtained after this subtraction, 5fC levels were designated as 0%. To call CpG sites with significant levels of 5fC, Fisher's exact test was performed to determine which CpG sites have significantly higher C signals in redBS-seq compared with BS-seq (FDR corrected P value less than 0.05). To calculate the level of 5caC, the level of 5fC measured by redBS-seq was subtracted from the level of 5fC + 5caC measured by MAB-seq, and negative values resulted from the subtraction were designated as 0%. To reduce the noise resulted from the two subtractions (one for 5fC calculation and one for 5caC calculation), uncalled sites in redBS-seq or MAB-seq were regarded as having 0% 5fC or 5fC+5caC, respectively.

Locus-specific caMAB-seq and 5caC calling. To perform locus-specific caMAB-seq, genomic DNA was first treated by M.SssI as described above and purified through PCI extraction. M.SssI-treated DNA was then reduced by $NaBH_4$ as described above in the redBS-seq protocol, followed by bisulfite conversion using Qiagen Epitect Bisulfite Kit. Selected loci were then amplified by PCR, and PCR amplicons were sequenced using Illumina deep sequencing. To examine whether unmodified C and 5fC are read as C during caMAB-seq, unmodified lambda DNA and synthesized 5fC oligo were also treated using the same protocol and analyzed by Illumina deep sequencing. In caMAB-seq, 5caC is read as T while C, 5mC, 5hmC and 5fC are read as C. To call 5caC-positive sites in a locus-specific caMAB-seq experiment, Fisher's exact test was performed to determine whether a CpG site in a sample has significantly higher percentage of T compared with background T signals detected in $Tet1/2^{-/-}$ sample. To calculate the absolute level of 5caC in a locus-specific experiment, the background signal detected in $Tet1/2^{-/-}$ sample was subtracted from the raw signal detected in a tested sample.

Genome-wide 5mC/5hmC/5fC/5caC DIP-seq. The antisera for 5fC and 5caC were previously described[39]. For each DIP experiment, 10 µg of sonicated, adaptor ligated genomic DNA from control or *Tdg* knockdown mouse ESCs (V6.5) was used as input, and 5 µl of 5mC antibody (Eurogentec, BI-MECY-0500), 5 µl of 5hmC antibody (Active Motif, 39791), 1 µl of 5fC antiserum or 0.3 µl of 5caC antiserum was added to immunoprecipitate modified DNA. DNA and antibodies were incubated at 4 °C overnight in a final volume of 500 µl DIP buffer (10 mM sodium phosphate (pH 7.0), 140 mM NaCl, 0.05% Triton X-100) as previously described[40]. After the DNA-antibody incubation, 30 µl of Protein G Dynabeads (Invitrogen) were added to the tube and incubated with the DNA-antibody mixture for 2 h at 4 °C. The beads were washed three times with 1 ml of DIP buffer, and then treated with proteinase

doi:10.1038/nbt.3073

K at 55 °C for 3 h to elute the immunoprecipitated DNA, which was further amplified for high-throughput sequencing.

Published data sets. For **Figure 2f** and **Supplementary Figure 8a**,**b**,**e**,**f**, we used following published data sets: Tet1 (Wu *et al.* 2011)[33], 5hmC base-resolution map[23], H3K4me3, H3K36me3, and H3K27me3 (ref. 28), H3K4me1 (ref. 41), Ezh2 (ref. 42), Oct4, Nanog, Sox2 [34], bivalent/active/silent promoters[43], LMR and UMR[44], H3K27ac and p300 (ref. 45), CTCF and tissue-specific enhancers[46], BNase, H2A.Z[31], H3.3, panH3 (ref. 32), and DNase I hypersensitive sites (ENCODE project)[47].

36. Bolger, A.M., Lohse, M. & Usadel, B. Trimmomatic: a flexible trimmer for Illumina sequence data. *Bioinformatics* **30**, 2114–2120 (2014).
37. Krueger, F. & Andrews, S.R. Bismark: a flexible aligner and methylation caller for Bisulfite-Seq applications. *Bioinformatics* **27**, 1571–1572 (2011).
38. Liu, Y., Siegmund, K.D., Laird, P.W. & Berman, B.P. Bis-SNP: combined DNA methylation and SNP calling for Bisulfite-seq data. *Genome Biol.* **13**, R61 (2012).
39. Inoue, A., Shen, L., Dai, Q., He, C. & Zhang, Y. Generation and replication-dependent dilution of 5fC and 5caC during mouse preimplantation development. *Cell Res.* **21**, 1670–1676 (2011).
40. Wu, H. *et al.* Genome-wide analysis of 5-hydroxymethylcytosine distribution reveals its dual function in transcriptional regulation in mouse embryonic stem cells. *Genes Dev.* **25**, 679–684 (2011).
41. Meissner, A. *et al.* Genome-scale DNA methylation maps of pluripotent and differentiated cells. *Nature* **454**, 766–770 (2008).
42. Ku, M. *et al.* Genomewide analysis of PRC1 and PRC2 occupancy identifies two classes of bivalent domains. *PLoS Genet.* **4**, e1000242 (2008).
43. Marson, A. *et al.* Connecting microRNA genes to the core transcriptional regulatory circuitry of embryonic stem cells. *Cell* **134**, 521–533 (2008).
44. Stadler, M.B. *et al.* DNA-binding factors shape the mouse methylome at distal regulatory regions. *Nature* **480**, 490–495 (2011).
45. Creyghton, M.P. *et al.* Histone H3K27ac separates active from poised enhancers and predicts developmental state. *Proc. Natl. Acad. Sci. USA* **107**, 21931–21936 (2010).
46. Shen, Y. *et al.* A map of the cis-regulatory sequences in the mouse genome. *Nature* **488**, 116–120 (2012).
47. ENCODE Project Consortium. An integrated encyclopedia of DNA elements in the human genome. *Nature* **489**, 57–74 (2012).

doi:10.1038/nbt.3073